



Oxidation Kinetics of a NiPtTi High Temperature Shape Memory Alloy

*James L. Smialek
Glenn Research Center, Cleveland, Ohio*

*Donald L. Humphrey
ASRC Aerospace Corporation, Cleveland, Ohio*

*Ronald D. Noebe
Glenn Research Center, Cleveland, Ohio*

NASA STI Program . . . in Profile

Since its founding, NASA has been dedicated to the advancement of aeronautics and space science. The NASA Scientific and Technical Information (STI) program plays a key part in helping NASA maintain this important role.

The NASA STI Program operates under the auspices of the Agency Chief Information Officer. It collects, organizes, provides for archiving, and disseminates NASA's STI. The NASA STI program provides access to the NASA Aeronautics and Space Database and its public interface, the NASA Technical Reports Server, thus providing one of the largest collections of aeronautical and space science STI in the world. Results are published in both non-NASA channels and by NASA in the NASA STI Report Series, which includes the following report types:

- **TECHNICAL PUBLICATION.** Reports of completed research or a major significant phase of research that present the results of NASA programs and include extensive data or theoretical analysis. Includes compilations of significant scientific and technical data and information deemed to be of continuing reference value. NASA counterpart of peer-reviewed formal professional papers but has less stringent limitations on manuscript length and extent of graphic presentations.
- **TECHNICAL MEMORANDUM.** Scientific and technical findings that are preliminary or of specialized interest, e.g., quick release reports, working papers, and bibliographies that contain minimal annotation. Does not contain extensive analysis.
- **CONTRACTOR REPORT.** Scientific and technical findings by NASA-sponsored contractors and grantees.
- **CONFERENCE PUBLICATION.** Collected papers from scientific and technical conferences, symposia, seminars, or other meetings sponsored or cosponsored by NASA.
- **SPECIAL PUBLICATION.** Scientific, technical, or historical information from NASA programs, projects, and missions, often concerned with subjects having substantial public interest.
- **TECHNICAL TRANSLATION.** English-language translations of foreign scientific and technical material pertinent to NASA's mission.

Specialized services also include creating custom thesauri, building customized databases, organizing and publishing research results.

For more information about the NASA STI program, see the following:

- Access the NASA STI program home page at <http://www.sti.nasa.gov>
- E-mail your question via the Internet to help@sti.nasa.gov
- Fax your question to the NASA STI Help Desk at 301-621-0134
- Telephone the NASA STI Help Desk at 301-621-0390
- Write to:
NASA Center for AeroSpace Information (CASI)
7115 Standard Drive
Hanover, MD 21076-1320



Oxidation Kinetics of a NiPtTi High Temperature Shape Memory Alloy

James L. Smialek
Glenn Research Center, Cleveland, Ohio

Donald L. Humphrey
ASRC Aerospace Corporation, Cleveland, Ohio

Ronald D. Noebe
Glenn Research Center, Cleveland, Ohio

National Aeronautics and
Space Administration

Glenn Research Center
Cleveland, Ohio 44135

Acknowledgments

This work was supported by the Supersonics Project of the NASA Fundamental Aeronautics Program.

This work was sponsored by the Fundamental Aeronautics Program
at the NASA Glenn Research Center.

Level of Review: This material has been technically reviewed by technical management.

Available from

NASA Center for Aerospace Information
7115 Standard Drive
Hanover, MD 21076-1320

National Technical Information Service
5285 Port Royal Road
Springfield, VA 22161

Available electronically at <http://gltrs.grc.nasa.gov>

Oxidation Kinetics of a NiPtTi High Temperature Shape Memory Alloy

James L. Smialek
National Aeronautics and Space Administration
Glenn Research Center
Cleveland, Ohio 44135

Donald L. Humphrey
ASRC Aerospace Corporation
Cleveland, Ohio 44135

Ronald D. Noebe
National Aeronautics and Space Administration
Glenn Research Center
Cleveland, Ohio 44135

Abstract

A high temperature shape memory alloy (HTSMA), Ni₃₀Pt₅₀Ti, with an M_s near 600 °C, was isothermally oxidized in air for 100 hr over the temperature range of 500 to 900 °C. Parabolic kinetics were confirmed by log-log and parabolic plots and showed no indication of fast transient oxidation. The overall behavior could be best described by the Arrhenius relationship:

$$k_p = 1.64 \times 10^{12} \exp\left[\frac{-250 \text{ kJ/mole}}{RT}\right] \text{mg}^2/\text{cm}^4\text{hr}$$

This is about a factor of 4 reduction compared to values measured here for a binary Ni₄₇Ti commercial SMA. The activation energy agreed with most literature values for TiO₂ scale growth measured for elemental Ti and other NiTi alloys. Assuming uniform alloy depletion of a 20 mil (0.5 mm) dia. HTSMA wire, ~1 percent Ti reduction is predicted after 20,000 hr oxidation at 500 °C, but becomes much more serious at higher temperatures.

1.0 Introduction

1.1 High Temperature Shape Memory Alloys

The shape memory effect has been associated with the thermoelastic martensitic transformation that occurs during cooling from a higher temperature parent phase (refs. 1 and 2). The thermoelastic nature of this transformation refers to the reversible transformation strain that occurs with successive temperature decrease. The shape memory effect occurs when deformation in the martensite regime is reversed by heating and transformation back to the parent phase, thus restoring the original undeformed shape. The special attributes of shape memory alloys and thermoelastic martensite were stated to be derived from internal twinning of the martensitic phase, and

possibly from ordered parent and daughter crystallographic structures (refs. 1 and 2). The internal twinning allows for shear stress-induced growth of one coherent twin variant over another, producing a macroscopic strain, without true plastic strain caused by dislocation movement. One role of the ordered phase prerequisite was thought to be the strengthening and resistance to dislocations that is normally associated with ordered phases. Another role is to require a specific single, symmetric crystallographic parent destination upon reheating from multiple, ordered, but less-symmetric, twin variant paths.

The shape memory phenomenon has been verified for a wide variety of alloys and compounds, e.g., AgCd, AuCd, CuAl, Fe-Ni, Fe₃Ti, Fe₃Pt, In-20Tl, Mn-15Cu (at.%), etc. The most prevalent shape memory alloy is the Ni₅₀Ti Nitinol material, which has found use in a number of medical, control (HVAC), and actuator applications. But all of these exhibit an M_s transformation temperatures near or below room temperature. Proposed turbine related devices, such as compact actuators for flow and clearance controls, moving or morphing inlet/exhaust configurations, and acoustic damping liners, all require some degree of higher temperature operation (ref. 3). To this end a multi-disciplinary, multi-organization program has been initiated to develop and characterize new HTSMA and engineer devices for commercial service under the recent NASA Fundamental Aeronautics Program.

Initial work has been focused on combining the SMA attributes of Ni₅₀Ti with the high transformation temperature enabled by Ti₅₀Pt (>1050 °C), since the ternary Ni-Pt-Ti system exhibits a linear relationship between M_s and percent Pt, figure 1 (refs. 4 and 5). For first generation turbine devices, it was anticipated that SMA effects would be needed in the 300 to 500 °C temperature range (ref. 6). Thus alloys of 20 and 30 at.% Pt were produced, corresponding to M_s of ~300 and ~600 °C, and studied with respect to transformation temperatures and hystereses, phase content and microstructure, recoverable strain, and transformation work output (refs. 7 and 8).

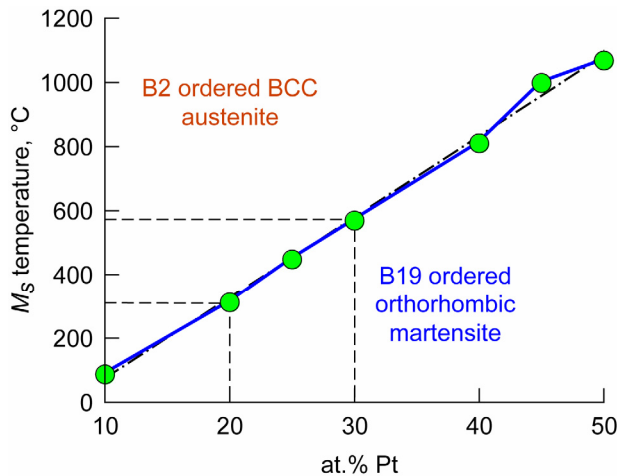


Figure 1.—The effect of Pt content on M_s transformation temperatures for $Ni_{50-x}Pt_xTi_{50}$ shape memory alloys, (after Noebe et al., ref. 5).

1.2 Oxidation of Ni-Ti Alloys

With regard to HTSMA, there is a specific concern that oxidative recession or alloy depletion may be significant due to the higher use temperatures. Although the binary Nitinol alloys are not designed for high temperature use, there have been a number of oxidation studies, with the idea being that SMA characteristics are modified by oxidation that occurs during hot rolling or that pre-oxidation may offer a stabilizing effect against corrosion for in vitro SMA devices, such as arterial stents.

First it is illustrative to provide a simplified overview from the broad perspective of thermodynamic stability and intrinsic kinetics in light of other commonly used protective scales, such as Al_2O_3 , Cr_2O_3 , and SiO_2 . Table 1 lists both the thermodynamic stability, given by the high temperature standard free energy of formation, and parabolic growth rate of NiO and TiO_2 scales compared to protective scales. It is seen that TiO_2 and Al_2O_3 have similar stabilities and would form in preference to the other oxides. However the growth rate of TiO_2 is orders of magnitude higher than all the remaining oxides, and would be expected to overtake any other scale. By comparison, NiO is the least stable oxide with 1/3 the free energy of TiO_2 , possessing a high growth rate, though still 600x lower than TiO_2 , and thus not expected to grow in competition with TiO_2 . Finally $PtO_2(v)$ has a positive free energy and only enters the kinetics as a volatile gaseous species, whose low equilibrium content $\sim 10^{-7}$ atm may be swept away from the surface, giving rise to a very slow linear weight loss that is usually ignored below 1100 °C.

These precepts are pointed out and verified by a number of the NiTi oxidation studies. Chan et al. oxidized NiTi for 1 hr at 450 °C and characterized the scale by AES and sputter profiling. They found primarily TiO_2 scales, with just a transient discontinuous mixture of NiO and TiO_2 in the outer 50 Å, and a depletion zone corresponding to $\sim Ni_2Ti$ (ref. 9).

Chu et al. (ref. 10) performed isothermal oxidation tests of NiTi in dry air for 6 hr at 550 to 1000 °C. They found TiO_2 scales, with a Ni_3Ti depletion zone and metallic Ni(Ti) trapped in an intermediate scale layer growing with a cellular structure at the higher temperatures. The overall kinetics were parabolic and yielded an activation energy of 226 kJ/mole. The B19' martensitic phase diminished with respect to the parent B2 phase with increasing oxidation temperature, presumably by depressing M_s below room temperature. While the authors attributed this to oxygen solution effects in the alloy, it would seem equally probable that preferential Ti oxidation and dilution may reduce M_s as discussed by Firstov et al. (ref. 11).

TABLE 1.—COMPARATIVE STABILITIES AND GROWTH RATES FOR NiTi OXIDATION AND COMMON PROTECTIVE SCALES

Oxide	$\Delta G_{1100^\circ C}$ (kcal/mole O_2)	$k_p, 1000^\circ C$ (mg^2/cm^4sec)
Al_2O_3	-197	6.14×10^{-14}
TiO_2	-167	6.13×10^{-8}
SiO_2	-152	1.73×10^{-14}
Cr_2O_3	-124	5.15×10^{-12}
NiO	-56	1.00×10^{-10}

$P_{r, 1000^\circ C} (PtO_2) \approx 4 \times 10^{-7}$ atm

They (ref. 11) oxidized NiTi for 30 hr at various temperatures and used a variety of surface analytical techniques. After 30 minutes of oxidation, XRD analysis revealed TiO at 300 to 500 °C, TiO_2 at 600 °C, adding NiO at 700 °C and $NiTiO_3$ at 800 °C. The B19' martensitic phase gave way to the B2 parent phase, with Ni_3Ti depletion zones increasing with temperature and a trace of elemental Ni, very near the gas surface, decreasing with temperature. Finally Xu et al. (ref. 12) have oxidized NiTi in oxygen for 4 hr at 450 to 750 °C and found parabolic kinetics at 550 °C and above, with an activation energy of 133 kJ/mole, resulting from primarily TiO_2 scale growth, with Ti-denuded internal oxidation and Ni_3Ti depletion zone layers. Partial spallation occurred after 750 °C oxidation, revealing somewhat of an open or porous interface and individual oxide crystallites.

Tian et al. (refs. 13 and 14) oxidized a high temperature Ni30Pd50Ti shape memory alloy at 900 °C for 46 hr in ambient air and found that 1 percent Ce additions prevented a discontinuity in the otherwise parabolic oxidation kinetics. They identified a lenticular oriented TiO_2 -rich outer scale, with an inner porous layer containing $NiTiO_3$ and Ti_4Pd_2O , with a 250 μm Ti depletion zone in the substrate causing a dramatic rise in hardness. These alloys oxidized somewhat slower than the binary NiTi and pure Ti.

The purpose of the present study is to characterize the oxidation behavior of the recently developed Ni-Pt-Ti high temperature shape memory alloy and compare it to that of a currently available commercial low temperature Ni-Ti SMA. In this paper the isothermal oxidation kinetics are emphasized, while the scale phases, chemistry, and microstructure will be presented in a subsequent companion paper. An ultimate goal

of the this paper will be to estimate oxidative consumption of the alloy in reference to geometric factors, alloy depletion level, and SMA performance.

2.0 Materials and Experimental Procedure

The conventional Ni47Ti Nitinol shape memory alloy was obtained commercially from Johnson Matthey Inc., in the form of 0.125 in. (3.18 mm) rolled plate which was then surface ground to 0.100 in. (2.54 mm) and EDM sectioned into 3/4 by 3/4 in. (1.9 by 1.9 cm) coupons. Chemical analysis of the Ni-47Ti alloy, performed by XRF (x-ray fluorescence), yielded Ni-49.3Ti-3.2Fe at.%. The Ni30Pt50Ti alloy was produced in our laboratory by vacuum induction melting in a graphite crucible, cast into a 1 in. dia. by 4 in. (2.54 dia. by 10.2 cm) long cylinder, and forged to 0.42 in. (1.07 cm), under a 1093 °C preheat. The plate was sectioned by electro-discharge machining (EDM) into 0.100 in. (2.54 mm) thick by 0.6 by 0.6 in. (1.5 by 1.5 cm) coupons. The primary alloy phase at room temperature was B19 ordered orthorhombic martensite, with an unintentional 2.1 vol% TiC dispersed particulate phase in the Ni30Pt50Ti material and an overall chemistry of 20.10 Ni, 49.66 Ti, 29.1 Pt, 0.85 C, 0.2 O, 0.06 N, and 0.02 Fe atom percent. Both alloy coupons were polished to a 600# grit finish with SiC emery paper and ultrasonically cleaned in detergent, then ethyl alcohol.

The samples were suspended from a Cahn 1000 thermogravimetric analysis (TGA) electrobalance by a sapphire hook attached to a Pt13Rh hanger wire and lowered into a vertical resistance furnace. The samples were oxidized in dried, bottled air, flowing at 100 cm³/min., at 500, 600, 700, and 800 °C for 100 hr, and at 900 °C for 10 hr. The weight change was recorded, corrected for buoyancy effects using a program tailored for graphical and statistical treatment of TGA kinetic data. The oxidized coupons were characterized by x-ray diffraction (XRD), scanning electron microscopy (SEM), and metallography, but these results will be presented in detail in a subsequent paper.

3.0 Results and Discussion

3.1 Thermogravimetric Response

The TGA weight gain curves for isothermal oxidation at 500 to 900 °C in air for 100 hr are shown in figure 2 for (a) Ni30Pt50Ti and (b) Ni47Ti. Reasonably well behaved curves are displayed with similar amplifications due to temperature, except that the abscissa for Ni47Ti is nearly twice that for Ni30Pt50Ti. In order to assess the rate law governing oxidation kinetics, the same data is presented as log weight gain versus log time in figure 3(a) and (b). The slopes of these plots show reasonable agreement with a time exponent of 0.5, shown as the dashed lines, according to the classic parabolic rate law,

$$\frac{\Delta W}{A} = \sqrt{k_p t} \quad (1)$$

Where ΔW is the change in mass, A is sample area, t is time, and k_p is the parabolic rate constant. The gravimetric data is then represented on parabolic plots in order to calculate $(k_p)^{1/2}$ values from the slopes of mass gain versus $t^{1/2}$ or to calculate k_p from the slope of (mass gain)² versus t curves. The former approach is summarized in figure 4, and, in general, linear relationships were displayed by both graphical techniques. In some instances, when the scale is expanded to show detail for each plot, an apparent divergence in the curve was observed.

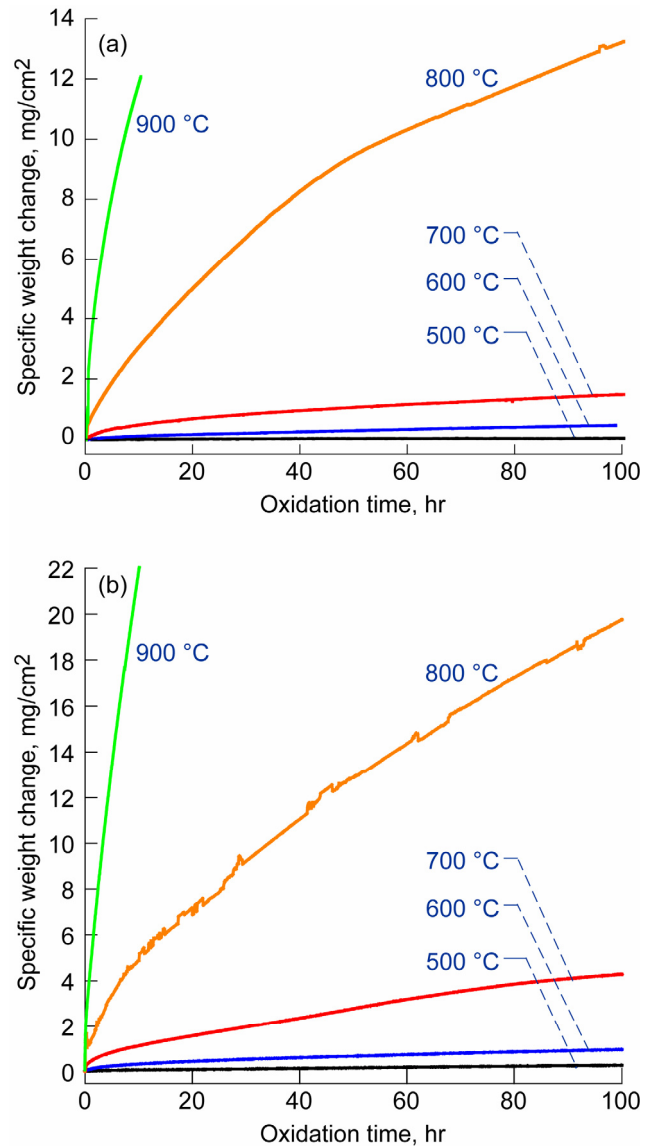


Figure 2.—The effect of temperature on the isothermal oxidation weight gain curves for Ni-Ti based shape memory alloys. (a) Ni30Pt50Ti. (b) Ni47Ti.

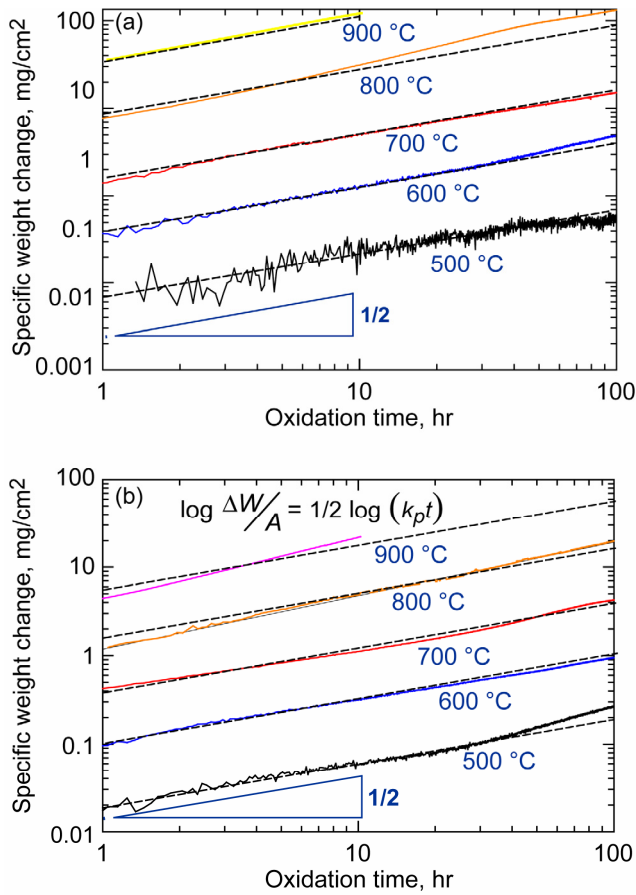


Figure 3.—Log-log plots of weight gain versus time for oxidation of Ni-Ti based shape memory alloys. (a) Ni30Pt50Ti. (b) Ni47Ti.

This led to the determination of both an initial and a final k_p , corresponding to the first 10 to 30 hr and then the remainder out to 100 hr, respectively. The overall results are listed in table 1 for both techniques, along with the $k_{p,avg}$ values determined over the entire oxidation time. The latter was applied to data beginning when the temperature reached within 100 °C of the oxidation temperature, usually within 3 min. of starting the run, and ending at the last minute of the run. However, the initial and final k_p values were determined over time ranges seen to have the most linear monotonic behavior, as shown for the dashed lines for the 800 °C data. For the most part, good regression fits were obtained, with r^2 of 0.99 or better, even though small inflections, curvature, or sigmoidal behavior could be discerned. The only poor r^2 values, obtained for fitting the Ni30Pt50Ti data at 500 °C, resulted from the large degree of noise relative to the small magnitudes of weight gain (only 0.06 mg/cm² total).

The general rule of thumb for choosing between $(\Delta W/A)$ versus $t^{1/2}$ or $(\Delta W/A)^2$ versus t parabolic constructions is that the former is preferred if fast growing transient oxides are formed, which do not contribute to subsequent rate control, while the latter is preferred if fast transients are formed that do

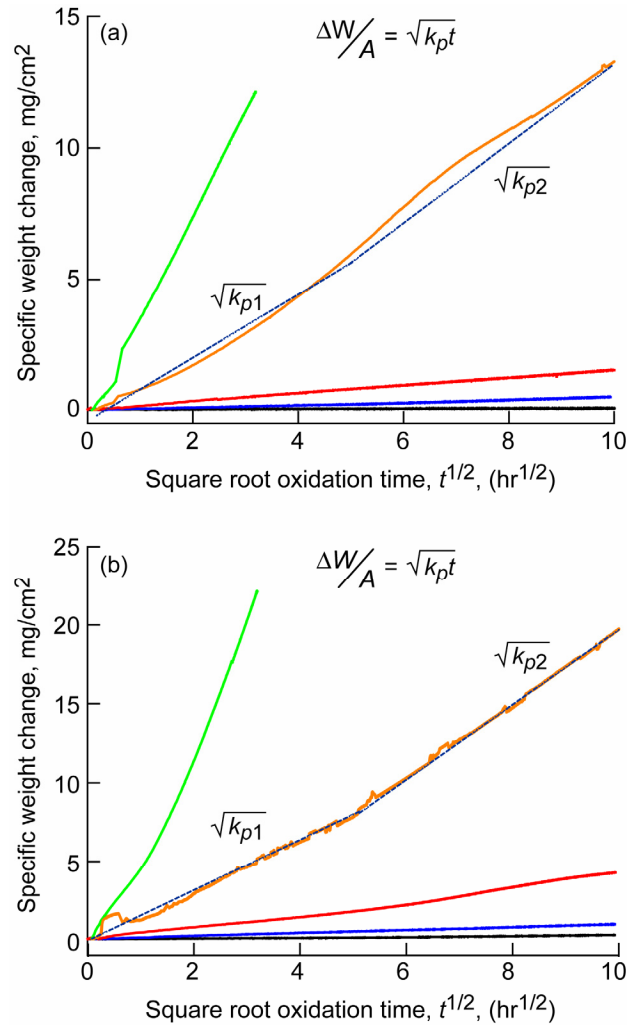


Figure 4.—Parabolic plots of weight gain versus $t^{1/2}$ for oxidation of Ni-Ti based shape memory alloys. (a) Ni30Pt50Ti. (b) Ni47Ti.

contribute to the final rate control (ref. 15). Apparently this was not an issue for these materials, since similar k_p values were determined by both types of plots. The k_p determined by the $t^{1/2}$ construction were nearly identical to those determined by $(\Delta W/A)^2$, table 1, and were compared by finding the ratio of the k_p determined by $t^{1/2}$ to that determined by $(\Delta W/A)^2$. For Ni30Pt50Ti the k_p ratio was 0.88 for both initial and final values, on average, and for Ni47Ti the ratios were 1.13 and 0.89 for the initial and final values, respectively.

3.2 Comparative Arrhenius Behavior

The k_p values obtained from table 1 were then plotted on an Arrhenius plot, figure 5. Here the initial and final k_p values are shown as downward and upward small triangle symbols, respectively. The larger symbols are more representative of overall behavior and were used to determine the linear relation between $\log k_p$ and $1/T$. Accordingly, the activation energy for

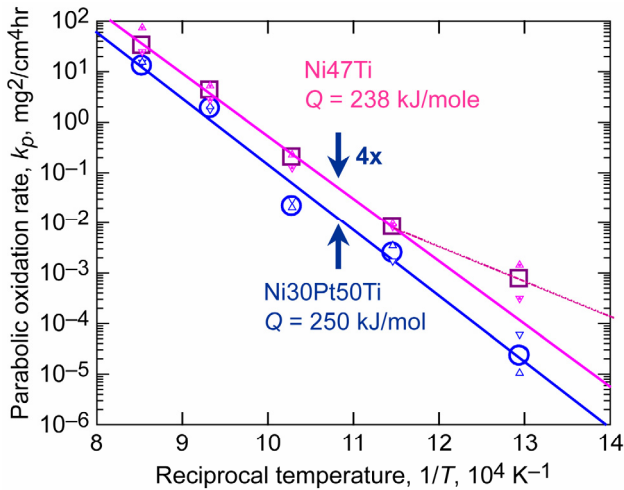


Figure 5.—Arrhenius plot of the average parabolic rate constant, showing similar activation energy for both alloys, but four times higher rates for Ni47Ti. (k_p , initial down triangles; k_p , final up triangles).

isothermal oxidation was determined to be ~250 kJ/mole for Ni30Pt50Ti and 238 kJ/mole for Ni47Ti. At 500 °C the Ni47Ti behavior appears to deviate from the higher temperature line and was therefore not included in the Arrhenius calculations. The remaining high temperature data indicated that the Ni30Pt50Ti rates were on average ~4.0x lower than those for the binary Ni47Ti alloy, using the best fit lines shown. Considering the spread in the data, these activation energies are not considered to be significantly different. The scale phases and microstructure will be discussed in the subsequent paper, but essentially show primary control by growth of TiO₂ rutile, with minor amounts of NiTiO₃.

The same construction was used to present the data from Xu, et al. (ref. 12) and Chu, et al. (ref. 10), figure 6, although these were obtained for only 4 and 6 hr total oxidation times, respectively, compared to primarily 100 hr used here. (It should be noted that the data from Chu et al. was modified from values presented on their $\ln k_p$ versus $1/T$ plot. This was done because the data from their mass gain versus time plots were not consistent with those on the \ln_e Arrhenius plot, rather they agreed with values if presented as a \log_{10} versus $1/T$ representation.) At the higher temperatures ≥ 700 °C, these data appear to be lower than those measured for the Ni47Ti alloy. Also, the linearized fit for data of the composite plot in Kofstad is shown for pure Ti, which includes mass gain from oxygen in solution in addition to external scale formation (ref. 17).

Linear regression was performed on the data sets for the five materials, and the resulting numerical relationships describing oxidation kinetics are listed in table 2. Here the pre-exponential 'A' term is presented both in terms of the convenient $\text{mg}^2/\text{cm}^4\text{hr}$ units, as well as in the cgs $\text{g}^2/\text{cm}^4\text{s}$ units. Four of the materials exhibit activation energies in the

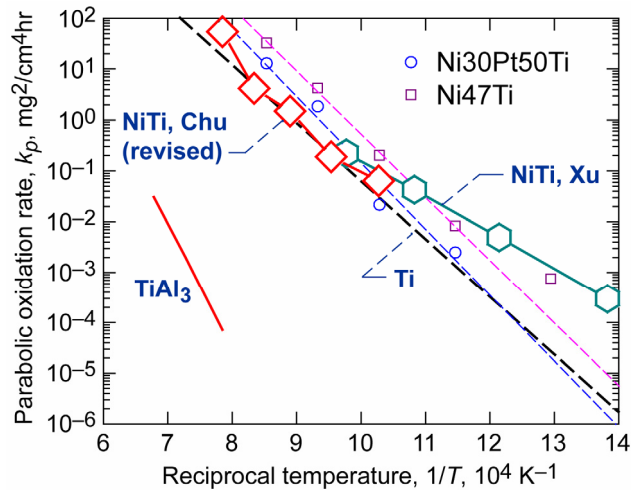


Figure 6.—Arrhenius plot comparing present data to the literature for NiTi, Ti, and TiAl₃ alloys.

range of 200 to 250 kJ/mole, which probably indicates rate control by the identical mechanism that controls Ti oxidation, namely TiO₂ growth, as previously proposed by Chu et al. (ref. 10). A related study (ref. 16) used scale thickness to present parabolic thickening kinetics and calculated an activation energy of 209 kJ/mole, again very much in agreement with TiO₂ control. The diversion of the 500 °C Ni47Ti and Xu data, the latter having an activation energy of only 136 kJ/mole, suggests deviation from this rate control at lower temperatures.

It is curious that, although the Ni30Pt50Ti data is systematically less than that of the Ni47Ti binary, both of the Ni-Ti alloys studied here oxidized somewhat faster than pure Ti. While it not uncommon for different experimental details and oxidation durations to shift a specific set of data, no explanation of this result is apparent.

Finally, it is shown that these Ti-containing alloys are ~5 orders of magnitude higher than TiAl₃, (ref. 18) which is known to form a slow growing $\alpha\text{-Al}_2\text{O}_3$ scale widely used for high temperature protection. From the standpoint of comparative long term oxidation resistance then, one might expect uncoated Ni-Ti alloys to be practical only in the 500 to 600 °C range.

3.3 Estimated Oxidative Life

Typically the oxidative life of high temperature structural materials is approached from the standpoint of reduction of useful cross-sectional area under load. Thus the time for a given amount of material recession due to oxidative consumption or the time to attain fast breakaway oxidation kinetics may be used to broadly define life. In the case of shape memory alloys, which must perform an additional, transformation-based function, life must also be envisioned as

the period of stable composition, as well as maintaining a useful cross-section. If oxidation consumes one alloying element preferentially, the transformation temperatures and phase stability may be seriously altered. In the case of Ni(Pt)Ti alloys, where Ti is preferentially removed by oxidation to form TiO₂ scales, this would initially have the effect reducing the M_s temperature and total work output of the transformation, introducing some second phase (Ni,Pt)-rich precipitates, or affecting mechanical properties. It is worth noting that a 1 percent drop in the Ti content of NiTi results in about a 90 °C reduction in M_s temperature.

The most critical geometrical consideration for oxidative failure is that of thin films or wires, where the ratio of

oxidative surface area to volume of Ti reservoir is the greatest. As an extreme example we consider the case of a wire, with radius r and length L . Here we intend to define the amount of Ti consumed in the scale, based on the isothermal rate constants, in terms of the change in at.% of Ti in the bulk of the wire. Equations (2) and (3) define the surface area and volume of a cylindrical wire or radius r , neglecting the end base surfaces. Equation (4) defines the mass of the wire in terms of the alloy density, which was found to be 10.5 g/cm³ from measurements of the mass and volume of the oxidation coupons:

$$A_{\text{wire}} = 2\pi rL \quad (2)$$

TABLE 2.—SUMMARY OF INITIAL AND FINAL PARABOLIC RATE CONSTANTS, $k_{p,(i \text{ or } f)}$, FOR Ni30Pt50Ti AND Ni47Ti SHAPE MEMORY ALLOYS. k_p DETERMINED FROM REGRESSION FITS OF (a) WEIGHT GAIN VERSUS $t^{1/2}$, (b) (WEIGHT GAIN)² VERSUS t PARABOLIC PLOTS

(a) Weight gain versus $t^{1/2}$										
Ni30Pt50Ti										
Temperature, °C	$k_{p,i}$	$k_{p,f}$	$k_{p,avg}$	Initial range, hr		Final range, hr		r_i^2	r_f^2	r_{avg}^2
500	6.24×10^{-5}	1.08×10^{-5}	2.69×10^{-5}	0.1	23.5	26.0	96.1	0.815	0.500	0.852
600	1.76×10^{-3}	3.55×10^{-3}	2.67×10^{-3}	0.1	20.5	29.1	94.9	0.994	1.000	0.990
700	3.02×10^{-2}	2.11×10^{-2}	2.21×10^{-2}	0.0	6.6	10.5	100	0.994	0.999	0.999
700*	-----	2.91×10^{-2}	-----	---	---	3.4	97.0	-----	1.000	-----
800	1.83×10^0	2.08×10^0	2.13×10^0	1.1	24.9	18.8	100	0.993	0.993	0.995
900	1.57×10^1	1.57×10^1	1.62×10^1	0.5	10.0	0.5	10.0	1.000	1.000	0.999
Ni47Ti										
Temperature, °C	$k_{p,i}$	$k_{p,f}$	$k_{p,avg}$	Initial range, hr		Final range, hr		r_i^2	r_f^2	r_{avg}^2
500	3.19×10^{-4}	1.46×10^{-3}	8.32×10^{-4}	0.1	29.0	39.4	96.9	0.986	0.996	0.968
600	8.45×10^{-3}	9.75×10^{-3}	8.62×10^{-3}	0.0	53.5	45.0	96.1	0.998	0.999	0.999
700	1.29×10^{-1}	2.33×10^{-1}	2.11×10^{-1}	0.0	39.0	46.4	86.9	0.996	0.999	0.986
700*	1.92×10^{-1}	2.34×10^{-1}	-----	0.95	26.45	42.3	95.0	0.997	0.997	-----
800	2.86×10^0	5.33×10^0	4.37×10^0	1.0	23.5	20.0	98.4	0.996	0.999	0.991
900	2.53×10^1	7.52×10^1	5.56×10^1	0.0	2.6	2.3	10.0	0.993	0.999	0.984
(b) Weight gain ² versus time										
Ni30Pt50Ti										
Temperature, °C	$k_{p,i}$	$k_{p,f}$	$k_{p,avg}$	Initial range, hr		Final range, hr		r_i^2	r_f^2	r_{avg}^2
500	4.59×10^{-5}	8.56×10^{-6}	2.84×10^{-5}	4.7	44.8	43.3	93.2	0.777	0.093	0.790
600	1.65×10^{-3}	2.85×10^{-3}	2.44×10^{-3}	0.3	30.5	45.6	96.6	0.999	0.994	0.988
700	2.46×10^{-2}	2.21×10^{-2}	2.25×10^{-2}	1.0	28.7	19.6	97.8	0.999	0.999	0.999
800	1.80×10^0	1.80×10^0	1.78×10^0	3.5	100.1	3.5	100.1	0.997	0.997	0.997
900	1.44×10^1	1.44×10^1	1.39×10^1	2.0	10.2	2.0	10.2	1.000	1.000	0.999
Ni47Ti										
Temperature, °C	$k_{p,i}$	$k_{p,f}$	$k_{p,avg}$	Initial range, hr		Final range, hr		r_i^2	r_f^2	r_{avg}^2
500	3.50×10^{-4}	9.34×10^{-4}	7.27×10^{-4}	2.0	34.4	43.9	98.4	0.976	0.994	0.967
600	8.70×10^{-3}	9.38×10^{-3}	8.92×10^{-3}	1.0	50.8	50.8	98.9	0.999	0.999	0.999
700	1.21×10^{-1}	3.00×10^{-1}	1.94×10^{-1}	0.9	30.3	30.3	97.2	0.998	0.998	0.988
800	2.73×10^0	4.05×10^0	3.65×10^0	4.1	40.8	30.2	98.4	0.984	0.998	0.988
900	4.17×10^1	5.86×10^1	4.87×10^1	1.6	5.0	4.6	10.1	0.995	0.998	0.982

*Duplicate run.

$$V_{\text{wire}} = \pi r^2 L \quad (3)$$

$$W_{\text{wire}} = \rho_{SMA} V \quad (4)$$

$$\rho_{SMA} = 10.5 \frac{\text{g}}{\text{cm}^3} \quad (5)$$

If Ti is assumed to be the primary alloy component consumed by oxidation, then the amount of Ti located in the TiO₂ scale may be equated with the Ti removed from the bulk, both normalized by unit area.

Since k_p refers only to the amount of oxygen weight gain, the amount of Ti in the scale is given by this amount of oxidation predicted from the parabolic rate constant, corrected by the ratio of the atomic weight of Ti, AW_{Ti} , to that of two oxygen atoms in TiO₂, MW_{O_2} , eq. (6):

$$\Delta W_{\text{Ti}}/A = \left(\frac{AW_{\text{Ti}}}{MW_{\text{O}_2}} \right) \sqrt{k_p t} \quad (6)$$

Whereas, the amount of Ti removed from the bulk is equivalent to the change in weight fraction of Ti, Δw_{Ti} , times the weight of the wire, normalized to unit area, eq. (7):

$$\Delta W_{\text{Ti}}/A = \Delta w_{\text{Ti}} \cdot \rho V/A \quad (7)$$

The change in weight fraction (Δw_{Ti}) is given by a prescribed change in atom fraction, Δat_{Ti} , as calculated from the usual at.% to wt.% conversions, eq. (8):

$$\Delta w_{\text{Ti}} \approx \frac{\Delta at_{\text{Ti}} \cdot AW_{\text{Ti}}}{\sum_{i=\text{Ni,Pt,Ti}} at_{\text{Ti}} \cdot AW_i} \quad (8)$$

For small changes in composition, this can be approximated by simply normalizing the change in Ti atom fraction, weighted by AW_{Ti} , to the sum of all the atom fractions weighted for each atom. (At larger changes in compositions, one should strictly calculate the change as (final wt. fraction) – (initial wt. fraction) by plugging in the specific initial and final atomic fractions determined for each element).

Equation (8) is then substituted in eq. (7), and the appropriate atomic weights and atom fractions for Ni30Pt50Ti are introduced. Accordingly, the mass per unit area of Ti removed from the bulk is determined and equated to that converted to oxide from eq. (6), yielding:

$$\sqrt{k_p t} = 1.78 r \cdot \Delta at_{\text{Ti}} \frac{\text{g}}{\text{cm}^3} \quad (9)$$

Thus the time to reduce the Ti content by a specified atom fraction can be estimated from the k_p (final) values measured here for any given wire radii. The results of such an exercise are given in table 3, assuming a wire radius of 10 or 22 mils (0.25 or 0.56 mm). For the 10 mil wire the oxidative life at 500 °C is over 18,000 hr for any compositional criterion allowing ≥ 1 at.% reduction in Ti content. The oxidative life increases as $(r \cdot \Delta at_{\text{Ti}})^2$, so for the larger wire with a radius of 22 mils, the time for 1 percent Ti reduction at 500 °C is now 91,000 hr. However, it is seen that this wide operational range is still limited to under 1000 hr at 600 °C. While it is thus expected that high temperature shape memory alloys based on

TABLE 3.—COMPARISON OF ACTIVATION ENERGIES AND PRE-EXPONENTIAL ARRHENIUS FACTORS (A, A') DETERMINED FROM PARABOLIC OXIDATION RATE CONSTANTS OF VARIOUS Ni-Ti ALLOYS

Alloy	A ($\text{mg}^2/\text{cm}^4\text{hr}$)	A' ($\text{g}^2/\text{cm}^4\text{s}$)	Q (kJ/mole)	Temperature, °C	Duration, hr	r^2	Reference
Ni30Pt50Ti	1.643×10^{12}	4.564×10^2	249.9	500 to 900	100	0.99	This study
Ni47Ti	1.399×10^{12}	3.886×10^2	237.9	600 to 900	100	1.00	This study
Ni50Ti	1.918×10^6	5.328×10^{-4}	135.7	450 to 750	4	1.00	Xu, et al. (2004)
Ni50Ti	4.853×10^{10}	1.274×10^1	224.8	700 to 1000	6	0.96	Chu, et al. (1996)
Ti	1.655×10^{10}	4.597×10^0	218.7	500 to 950	N/A	N/A	Kofstad (1988)

TABLE 4.—ESTIMATED OXIDATIVE LIFE FOR A 10 mil (0.010 in.) AND 22 mil RADIUS (0.022 in.) WIRE AS A FUNCTION OF TEMPERATURE AND ALLOWABLE COMPOSITIONAL (ATOM FRACTION Ti) LOSS

Temperature, °C	$r = 10$ mils (254 μm)			$r = 22$ mils (559 μm)		
	$\Delta at_{\text{Ti}} = 0.01$, hr	0.05 Ti, hr	0.10 Ti, hr	0.01 Ti, hr	0.05 Ti, hr	0.10 Ti, hr
500	18927	473177	1892708	91607	2290177	9160708
600	57.6	1440	5758	279	6967	27869
700	9.7	242	969	46.9	1172	4689
800	0.10	2.5	10	0.48	11.9	48
900	0.01	0.33	1.3	0.06	1.6	6

the Ni-Ti system will be able to function reasonably well from an oxidation standpoint, some caution must be exercised for exposures exceeding 500 °C.

One final issue is that of composition gradient. Since the bulk composition in these calculations was assumed to be uniform, any effects of the expected depletion zone are not accounted for here. These may include a more severe response due to the more greatly affected surface composition, with the opposing factor of a less severely affected bulk composition.

The exact nature of the gradient, SMA behavior, and device application would be needed to predict these effects more intelligently, and SMA behavior should be measured directly as a function of oxidation. More conservative estimates can be expected when more aggressive, realistic test factors, such as thermal cycling (e.g., see scale spallation below) or thermomechanical fatigue, are addressed.

3.4 Scale Spallation

Although not intended to study cyclic effects, such as repeated scale spallation and regrowth, some of the isothermal tests established such thick scales that even one cool down cycle was enough to cause severe spallation. This was initially apparent simply from visual observations, as confirmed by the macrographs of figure 7. While little evidence of spallation is present for Ni₃₀Pt₅₀Ti samples oxidized at 700 °C or below, massive delamination of broad plateaus of scale is apparent for the 800 and 900 °C samples. Similarly the Ni₄₇Ti sample oxidized at 600 °C appears relatively intact, whereas those oxidized at all the remaining higher temperatures exhibit broad areas of delamination. While this spalling morphology indicated substantial thickness or depth of the spalled region, spallation to bare metal was not observed. The relative amount of scale spalled is shown for each macrograph, as obtained by the following analysis.

The weight gain from the TGA apparatus yields the maximum (oxygen) weight gain at the end of the exposure. The difference in cooled weight versus starting weight yields the net sample weight change. If no spalling occurred, the net sample change should equal that measured as the TGA gain. If it is lower than the TGA gain, the difference should represent spalled weight of oxide. The mass of spalled scale is presented in figure 8 as the dashed lines and are compared to the solid lines for the maximum gain in the TGA apparatus, both for Ni₃₀Pt₅₀Ti (fig. 8(a)) and for Ni₄₇Ti (fig. 8(b)). Minimal spallation is confirmed for Ni₃₀Pt₅₀Ti at 700 °C and below, as is the excessive spallation at 800 and 900 °C. Similarly, small but measurable spallation occurred for Ni₄₇Ti at 700 °C, which then became extreme at 800 and 900 °C. (The amount of spallation at 900 °C would be further increased if samples were oxidized for the full 100 hr rather than just 10 hr here.)

The overall increase in the amount of spallation with oxidation temperature can be viewed as a result of both increased scale thickness and the larger temperature

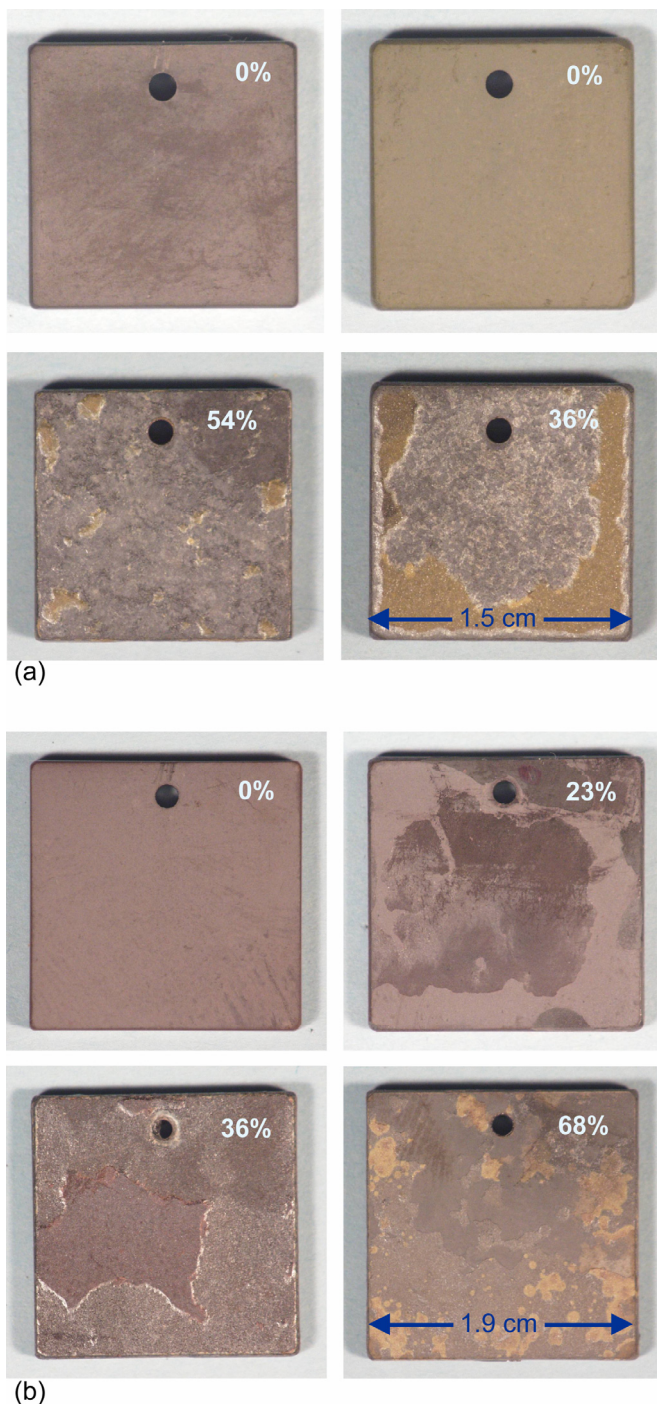


Figure 7.—Macrographs of Ni-Ti based shape memory alloys showing spallation estimates (percent) after 100 hr oxidation at 600, 700, 800, and after 10 hr at 900 °C. (a) Ni₃₀Pt₅₀Ti. (b) Ni₄₇Ti.

differential over which thermal expansion mismatch stresses will accrue. For example, the thermal expansion of TiO₂ is approximately 6.8 to $8.3 \times 10^{-6}/^{\circ}\text{C}$, compared to about $10 \times 10^{-6}/^{\circ}\text{C}$ and 7 to $11 \times 10^{-6}/^{\circ}\text{C}$ for NiPtTi and NiTi alloys,

respectively. Thus compressive buckling stresses will be built up in the scale, as with most oxidized metals, but this thermal expansion mismatch stress would not be expected to be any higher for the NiTi alloy, which showed some increased propensity for spallation.

It is noted that at some temperatures the mass of oxide spallation exceeds that of oxygen gain for both alloys. This may be explained by the theoretical maximum ratio of total TiO₂ spall to total O₂ gain (2.497), given by their respective molecular weights, if all the scale were removed. One can estimate the fraction of scale spalled using this stoichiometric factor, assuming the scale is 100 percent TiO₂. Thus, in table 5 and in figure 8, it is seen that the fraction spalled reached 35 to 55 percent for the Ni30Pt50Ti alloy and 23 to 70 percent for the Ni47Ti binary. Although these represent extremely high values, especially considering any cyclic exposure at extreme temperatures, they are not 100 percent and therefore below the theoretical maximum for total spallation. This is consistent with the absence of any obvious bare metal spallation. In any event, this analysis is presented for general behavior, and spalling values should not be taken as absolute. For example, the relatively low amount of oxidation at low temperatures amplifies any discrepancies between oxygen gain measured in the TGA compared to oxide spalled measured externally by laboratory bench analytical microbalances. (On occasion, a negative amount of spallation is calculated, with no physical meaning). Furthermore, handling and hang wire trapped in the hanger hole (Ni47Pt at 800 °C) are expected to introduce some error.

While scale spallation will be an important phenomenon regarding future overall life prediction schemes, it appears to be less of an issue for the Ni30Pt50Ti alloy below 800 °C, i.e., well above any intended use temperature.

4.0 Summary and Concluding Remarks

Ni30Pt50Ti and Ni47Ti shape memory alloys were isothermally oxidized in air for 100 hr over the temperature range of 500 to 900 °C. Parabolic kinetics were confirmed by log-log and by $\Delta W/A$ versus $t^{1/2}$ or $(\Delta W/A)^2$ versus t parabolic plots, showing no indication of fast transient oxidation. However, somewhat improved fits to the experimental data were obtained by using an initial and final rate constant,

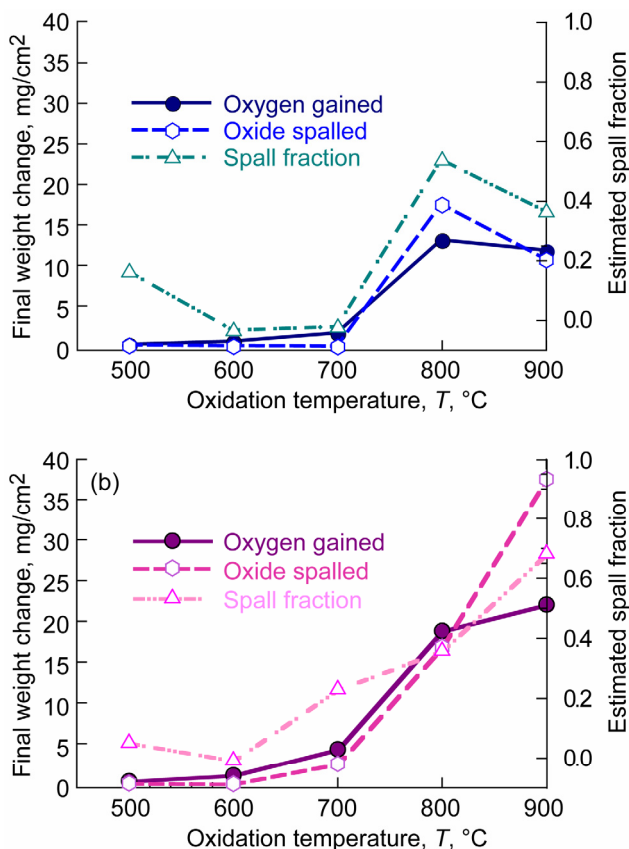


Figure 8.—The effect of oxidation temperature on the total weight of oxygen gained, calculated weight of scale spalled, and estimated weight fraction of scale spalled, shown here to exceed 50 percent at the higher temperatures. (a) Ni30Pt50Ti. (b) Ni47Ti.

generally over the first 30 hr and final 70 hr, respectively. The overall behavior could be best described by the Arrhenius relationships:

for Ni30Pt50Ti

$$k_p = 1.64 \times 10^{12} \exp[(-250 \text{ kJ/mole})/RT] \text{ mg}^2/\text{cm}^4\text{hr}$$

and for Ni47Ti

$$k_p = 1.40 \times 10^{12} \exp[(-238 \text{ kJ/mole})/RT] \text{ mg}^2/\text{cm}^4\text{hr}$$

TABLE 5.—SPALL FRACTION ESTIMATED FROM MAXIMUM TGA WEIGHT GAIN AND NET SAMPLE WEIGHT CHANGE, ASSUMING A TiO₂ SCALE

Time, hr	Temperature, °C	Ni30Pt50Ti			Ni47Ti		
		Max O ₂ gain mg/cm ²	Total spall mg/cm ²	Spall fraction	Max O ₂ gain mg/cm ²	Total spall mg/cm ²	Spall fraction
100	500	0.11	0.04	0.16	0.32	0.04	0.05
100	600	0.49	-0.04	-0.04	1.04	-0.02	-0.01
100	700	1.53	-0.09	-0.02	4.30	2.47	0.23
100	800	13.02	17.43	0.54	18.82	16.85	0.36
10	900	11.74	10.64	0.36	22.06	37.55	0.68

resulting in about a factor of 4 lower k_p for the ternary alloy compared to NiTi. Analogous to the Ni30Pd50Ti study by Tian et al. (refs. 13 and 14), one may expect the massive Pt atoms to reduce overall diffusion rates in the alloy and curtail the supply of Ti to the scale somewhat. Extrapolation of these relations to lower temperatures appears warranted for the Ni30Pt50Ti alloy, but not for NiTi. While the activation energies above agreed with the oxidation of elemental Ti and one NiTi study from the literature, another NiTi study, conducted in oxygen, yielded an activation energy of only 136 kJ/mole, or about half the other values. This may be explained as a possible break in the Arrhenius behavior for the lower temperatures. Furthermore, even at higher temperatures in air, there remains a slight difference between the previously published NiTi values and those measured here.

While spallation is an important issue for life prediction, and becomes quite apparent at 700 °C and above, reaching values over 50 percent of the scale, cyclic tests were not part of this study. Based on the scale thicknesses achieved, spallation is expected to be minimal for cyclic tests at 500 °C or below, as is being born out in some preliminary testing. Based on uniform alloy depletion, the oxidative life of a HTSMA wire component is estimated to vary inversely with k_p and with $(r_{\text{wire}}\Delta t_{\text{Ti}})^2$, where Δt_{Ti} is the allowable atom fraction of Ti consumed. For a 20 mil dia. HTSMA wire, a 1 percent Ti reduction is expected after almost 20,000 hr at 500 °C. However, serious depletion can be expected for much shorter times if the HTSMA wire were to be oxidized at higher temperatures.

References

1. C.M. Wayman and K. Shimizu, "The Shape Memory ("Marmem") Effect in Alloys, *Metal Science Journal*, **6**, p. 175 (1972).
2. *Shape Memory Materials*, edited by K. Otsuka and C.M. Wayman, Cambridge University Press, Cambridge, U.K., 1998.
3. R.D. Noebe, T. Biles, and S.A. Padula, "Chapter 7: NiTi-Based High-Temperature Shape-Memory Alloys: Properties, Prospects, and Potential Applications," in *Advanced Structural Materials: Properties, Design Optimization, and Applications*, W.O. Soboyejo, Ed., Taylor & Francis Group, Boca Raton, FL, 2006, pp. 141–180.
4. P.G. Lindquist and C.M. Wayman, "Shape Memory and Transformation Behavior of Martensitic Ti-Pd-Ni and Ti-Pt-Ni Alloys," in *Engineering Aspects of Shape-Memory Alloys*, Duerig, T.W., Melton, K.N., Stockel, D., and Wayman, C.M., Eds., Butterworth-Heinemann, London, pp. 58–68, 1990.
5. O. Rios, R. Noebe, T. Biles, A. Garg, A. Palczer, D. Scheiman, H.J. Seifert, M. Kaufman, "Characterization of Ternary NiTiPt High-Temperature Shape Memory Alloys," in *Smart Structures and Materials 2005: Active Materials: Behavior and Mechanics*, SPIE Conf. Proc. Vol. 5761, (2005), pp. 376–387.
6. J.A. DeCastro, K.J. Melcher, R.D. Noebe, "System-Level Design of a Shape Memory Alloy Actuator for Active Clearance Control in the High-Pressure Turbine," in Proceedings of the 41st Joint Propulsion Conference and Exhibit, American Institute of Aeronautics and Astronautics, Paper AIAA–2005–3988, (2005).
7. R. Noebe, D. Gaydosh, S. Padula, A. Garg, T. Biles, and M. Nathal, "Properties and Potential of Two (Ni,Pt)Ti Alloys for Use as High-Temperature Actuator Materials," in *Smart Structures and Materials 2005: Active Materials: Behavior and Mechanics*, SPIE Conf. Proc. vol. 5761, (2005), pp. 364–375.
8. R. Noebe, S. Draper, D. Gaydosh, A. Garg, B. Lerch, Nicholas, Penney, G. Bigelow, S. Padula, and J. Brown, "Effect of Thermomechanical Processing on the Microstructure, Properties, and Work Behavior of a Ti_{50.5}Ni_{29.5}Pt₂₀ High-Temperature Shape Memory Alloy," in SMST 2006: Proceedings of the International Conference on Shape Memory and Superelastic Technologies, ASM International, Metals Park, OH, (2007).
9. C.M. Chan, S. Trigwell, T.W. Duerig, "Oxidation of an NiTi Alloy," *Surface and Interface Analysis*, **5**, pp. 349–354 (1990).
10. C.L. Chu, S.K. Wu, Y.C. Yen, "Oxidation behavior of equiatomic TiNi alloy in high temperature air environment," *Materials Science and Engineering*, **A 216**, pp. 193–200 (1996).
11. G.S. Firstov, et al., "Surface oxidation of NiTi shape memory alloy," *Biomaterials*, **23**, pp. 4863–4871 (2002).
12. C.H. Xu, X.Q. Ma, S.Q. Shi, C.H. Woo, "Oxidation behavior of TiNi shape memory alloy at 450–750 °C," *Materials Science and Engineering*, **A 371**, pp. 45–50 (2004).
13. Q. Tian and J. Wu, "Effect of the Rare Earth Element Ce on Oxidation Behavior of TiPdNi Alloys," *Materials Science Forum*, **394–395**, pp. 455–458 (2002).
14. Q. Tian, J. Chen, Y. Chen, and J. Wu, "Oxidation behavior of TiNi-Pd shape memory alloys," *Z. Metallkde.*, **94**, pp. 36–40 (2003).
15. B. Pieraggi, "Calculations of Parabolic Reaction Rate Constants," *Oxidation of Metals*, **27**, pp. 177–185 (1987).
16. L. Zhu, J.M. Fino, and A. Pelton, "Oxidation of Nitinol," *Shape Memory and Superelastic Technology Proceedings*, SMST–2003, eds. T.W. Duerig and A. Pelton, SMST–ASM International, Metals Park, OH (2003).
17. P. Kofstad, *High Temperature Corrosion*, Elsevier Applied Science, London, 1988, p. 293.
18. J. L. Smialek and D. L. Humphrey, "Oxidation Kinetics of Cast TiAl₃," *Scripta Met. et Mat.*, **26**, pp. 1763–1768 (1992).

REPORT DOCUMENTATION PAGE

Form Approved
OMB No. 0704-0188

The public reporting burden for this collection of information is estimated to average 1 hour per response, including the time for reviewing instructions, searching existing data sources, gathering and maintaining the data needed, and completing and reviewing the collection of information. Send comments regarding this burden estimate or any other aspect of this collection of information, including suggestions for reducing this burden, to Department of Defense, Washington Headquarters Services, Directorate for Information Operations and Reports (0704-0188), 1215 Jefferson Davis Highway, Suite 1204, Arlington, VA 22202-4302. Respondents should be aware that notwithstanding any other provision of law, no person shall be subject to any penalty for failing to comply with a collection of information if it does not display a currently valid OMB control number.

PLEASE DO NOT RETURN YOUR FORM TO THE ABOVE ADDRESS.

1. REPORT DATE (DD-MM-YYYY) 17-04-2007		2. REPORT TYPE Technical Memorandum		3. DATES COVERED (From - To)	
4. TITLE AND SUBTITLE Oxidation Kinetics of a NiPtTi High Temperature Shape Memory Alloy				5a. CONTRACT NUMBER	
				5b. GRANT NUMBER	
				5c. PROGRAM ELEMENT NUMBER	
6. AUTHOR(S) Smialek, James, L.; Humphrey, Donald, L.; Noebe, Ronald, D.				5d. PROJECT NUMBER	
				5e. TASK NUMBER	
				5f. WORK UNIT NUMBER WBS 561581.02.08.03.15.03	
7. PERFORMING ORGANIZATION NAME(S) AND ADDRESS(ES) National Aeronautics and Space Administration John H. Glenn Research Center at Lewis Field Cleveland, Ohio 44135-3191				8. PERFORMING ORGANIZATION REPORT NUMBER E-15898	
9. SPONSORING/MONITORING AGENCY NAME(S) AND ADDRESS(ES) National Aeronautics and Space Administration Washington, DC 20546-0001				10. SPONSORING/MONITORS ACRONYM(S) NASA	
				11. SPONSORING/MONITORING REPORT NUMBER NASA/TM-2007-214697	
12. DISTRIBUTION/AVAILABILITY STATEMENT Unclassified-Unlimited Subject Categories: 25 and 26 Available electronically at http://gltrs.grc.nasa.gov This publication is available from the NASA Center for AeroSpace Information, 301-621-0390					
13. SUPPLEMENTARY NOTES					
14. ABSTRACT A high temperature shape memory alloy (HTSMA), Ni ₃₀ Pt ₅₀ Ti, with an M_s near 600 °C, was isothermally oxidized in air for 100 hr over the temperature range of 500 to 900 °C. Parabolic kinetics were confirmed by log-log and parabolic plots and showed no indication of fast transient oxidation. The overall behavior could be best described by the Arrhenius relationship: $k_p = 1.64 \times 10^{12} \exp[(-250 \text{ kJ/mole})/RT]$ mg ² /cm ⁴ hr. This is about a factor of 4 reduction compared to values measured here for a binary Ni ₄₇ Ti commercial SMA. The activation energy agreed with most literature values for TiO ₂ scale growth measured for elemental Ti and other NiTi alloys. Assuming uniform alloy depletion of a 20 mil (0.5 mm) dia. HTSMA wire, ~1 percent Ti reduction is predicted after 20,000 hr oxidation at 500 °C, but becomes much more serious at higher temperatures.					
15. SUBJECT TERMS Oxidation; Kinetics; High temperature materials; Nickel; Platinum; Titanium; Martensite; Shape memory alloys; Titanium oxide					
16. SECURITY CLASSIFICATION OF:			17. LIMITATION OF ABSTRACT	18. NUMBER OF PAGES 16	19a. NAME OF RESPONSIBLE PERSON James L. Smialek
a. REPORT U	b. ABSTRACT U	c. THIS PAGE U			19b. TELEPHONE NUMBER (include area code) 216-433-5500

